Infrared emittance of Cu_x–Ni_{1-x} alloys

2004 J. Phys.: Condens. Matter 16 833

(http://iopscience.iop.org/0953-8984/16/6/013)

INSTITUTE OF PHYSICS PUBLISHING JOURNAL OF PHYSICS: CONDENSED MATTER

J. Phys.: Condens. Matter **16** (2004) 833–843 PII: S0953-8984(04)71632-X

Infrared emittance of Cu_x–Ni_{1-x} alloys

K Gelin[1] **and E Wäckelgård**

Division of Solid State Physics, Department of Engineering Sciences, Uppsala University, Box 534, SE-751 21 Uppsala, Sweden

E-mail: Kristina.Gelin@angstrom.uu.se

Received 10 November 2003
Published 30 January 2004
Online at stacks.iop.org/JPhysCM/16/833 (DOI: 10.1088/0953-8984/16/6/013)

Abstract

The aim of this work was to study Cu–Ni alloys and establish a relation between alloy concentration and infrared emittance for wavelengths of the order 10 μm, which is of interest in room temperature applications. The resistivity was measured at room temperature for the same alloy compositions as the emittance in order to investigate the validity of the Hagen–Rubens relation in the infrared wavelength range for Cu–Ni. The Hagen–Rubens relation is verified for both the copper-rich and nickel-rich samples. We therefore assume strong electron scattering from impurities so that intraband transitions dominate over interband transitions in the infrared wavelength range. The validity of the Hagen–Rubens relation can, as a good approximation, also be used for the integrated thermal emittance.

1. Introduction

The aim of this work was to study the infrared emittance of Cu–Ni alloys. Infrared emittance of metals is of interest in thermal radiant applications such as heat mirrors and spectrally selective solar absorbers. Alloys are of interest in applications where the surface is exposed to harsh chemical conditions.

The copper–nickel alloy has been the subject of considerable theoretical and experimental work and has been taken as the prototype of noble-metal–transition-metal systems since it has the advantage of being solid soluble over the entire compositional range. Comparing electron band structures of Ni and Cu shows that the s–p bands are very similar but not the 3d bands [1]. The location of the 3d bands is well below the Fermi level in Cu and at the Fermi level in Ni. The electron band structure of the Cu–Ni alloys was first described in terms of the rigid band model, which could accurately predict the Ni concentration limit of about 40% above which the alloy is ferromagnetic [2]. Later on, the rigid band model was opposed by results from measurements of optical absorption [3–6], ellipsometry [7], electron emission [4, 5] and soft

[1] Author to whom any correspondence should be addressed.

x-ray emission [8]. Virtual bound state (VBS) models [9, 10] were proposed for the dilute systems [3, 11] and the coherent potential approximation (CPA) (in which the VBS is a low concentration limit) for concentrated systems [7, 12–14]. To summarize, the review indicates that the rigid band model is abandoned in favour of the CPA. According to the CPA model Cu preserves its d-band states well below the Fermi level for all concentrations, while the nickel 3d states show up as virtual bound states between the high energy edge of the Cu 3d states and the Fermi energy. The Ni 3d states then broaden and extend to the Fermi level for increasing concentration of Ni in the system.

Pure Cu shows interband dominated optical absorption for energies above 2 eV and intraband dominated absorption for lower energies, leading to a constant reflectance in the infrared wavelength range [15]. It shows the behaviour of a Drude metal in the relaxation interval for which the frequency is higher than the inverse relaxation time but lower than the plasma frequency [16]. Nickel is a transition metal, not a free electron metal, due to d-band states at the Fermi level that give interband dominated optical absorption in the infrared region [17]. It has been found from analysis of optical absorption in copper-rich Cu–Ni alloys that the characteristic absorption edge in Cu at 2.1 eV, which is due to interband transitions between 3d states and the Fermi level, loses sharpness but can be distinguished for concentrations of 5–75% Cu. In addition a sharp absorption band appears at about 1 eV for concentrations above of 5–65% Cu [18]. The wavelength dependence of the optical absorption in nickel-rich Cu–Ni behaves more like the absorption in pure nickel [5, 18]. However, the question is whether a free carrier contribution (intraband transitions), in the alloys, in any case dominates in the infrared due to strong impurity scattering. It has been shown for Cu with 1 at.% Ni that $\hbar/\tau = 0.02$ eV, where τ is the relaxation time, for pure Cu $\hbar/\tau$ was increased to 0.71 eV [19]. Converted to time, these values correspond to relaxation times of about 3×10^{-14} and 9×10^{-16} s respectively. The short relaxation time in $Cu_{99}Ni_1$ could lead to intraband transitions taking over as the dominating absorption mechanism in the infrared range. A relaxation time of this order is short enough to fulfil the condition in the low frequency limit in the Drude model for which the frequency is larger than the inverse relaxation time. It has also been reported that the zero-frequency limit of the optical conductivity has a similar dependence on alloy concentration as the dc conductivity in the whole concentration range [18], which then also indicates that intraband absorption dominates for low frequencies.

The emittance was derived from reflectance measurements over the whole compositional range with the purpose of establishing a relation between alloy concentration and infrared emittance for wavelengths of the order of 10 μm, which is of interest in room temperature applications. If the intraband absorption dominates and the infrared wavelength range around 10 μm can be considered as the low frequency range according to the Drude theory, we would expect the emittance to change with composition in a similar manner as the dc electrical resistivity since these two entities are related according to the Hagen–Rubens relation [2]. In alloys, the dc electrical resistivity shows a gradual increase for increased concentration of one of the constituents in the alloy and it reaches a maximum value at about equal concentration of both. The resistivity can be described by the Nordheim rule for noble metals with similar atomic volumes and the same valence and crystal structure [2]. The resistivity and emittance were measured at room temperature for identical alloy compositions in order to investigate the validity of the Hagen–Rubens relation in the infrared range in Cu–Ni.

2. Theorical framework

The Hagen–Rubens relation is usually expressed as the spectral reflectance $R(\omega)$ at normal angle of incidence as a function of the frequency ω [2]:

$$R(\omega) = 1 - 2\left[\frac{2\varepsilon_0\omega}{\sigma_0}\right]^{1/2} \tag{1}$$

where σ_0 is the dc-electrical conductivity and ε_0 the vacuum permittivity. The dc-electrical conductivity for a metal, according to the Drude model, depends on the free electron concentration n_e, the relaxation time τ and the effective electron mass m^* [20]:

$$\sigma_0 = \frac{n_e e^2 \tau}{m^*}. \tag{2}$$

The dominating contribution to the relaxation time is assumed to be impurity scattering in the Cu–Ni alloys. Considering also that the scattering comes from neutral impurities the relaxation time should be frequency independent [21], which is required for the Hagen–Rubens relation. Substituting reflectance for emittance ε (valid for bulk metals) and the electrical conductivity with the inverse of the electrical resistivity ρ, equation (1) can be expressed as the emittance as a function of wavelength λ ($\lambda = 2\pi c/\omega$, where c is the light velocity in vacuum):

$$\varepsilon = 2\left[\frac{4\pi\varepsilon_0 c\rho_0}{\lambda}\right]^{1/2}. \tag{3}$$

3. Sample preparation

Seven different bulk copper–nickel alloys and a copper and a nickel sample were manufactured by Metalli AB, Denmark. The samples were ordered in weight per cent but the element content will from now be used in atomic per cent. The ordered alloys had the following concentrations: Cu_9Ni_{91}, $Cu_{28}Ni_{72}$, $Cu_{38}Ni_{62}$, $Cu_{48}Ni_{52}$, $Cu_{58}Ni_{42}$, $Cu_{68}Ni_{32}$ and $Cu_{89}Ni_{11}$. The copper and the nickel samples have a purity of 99.9%. The purities of the elements in the alloy samples are 99.99% for copper and 99.94% for nickel. The manufacturer reported the alloy content of the samples with the uncertainty of one percentage point.

According to the manufacturer the alloys were made in an induction vacuum furnace at different temperatures, depending on the alloy, within 150° from the exact temperature of the liquid. The melt was naturally cooled in the furnace until the temperature was below 473 K.

To verify that the copper and nickel were in a complete solid solution and no other phases were present in the samples, the samples were checked with x-ray diffraction.

The samples used for the reflectance measurements were manually polished with a water-cooled Buehler® ECOMET® 2 (two-speed grinder-polisher), with silicon carbide grinding papers. The abrasive particle sizes ranged from 220 grit (65 μm) to 4000 grit (1–5 μm). To remove any thin oxide layer, the sample surfaces were dipped in a weak solution of sulfuric acid, rinsed in de-ionized water and dried with a flow of nitrogen gas, before the optical measurements.

Small rods were cut out from the polished bulk samples for the resistivity measurements. The rods were then ground, with the polisher mentioned previously, to cut thin rods. Finally, a Buehler® ISOMET™ low speed saw equipped with a diamond wafer was used to achieve proper lengths of the rods. The typical dimensions of an alloy sample for resistivity measurements were 20 mm × 0.6 mm × 0.3 mm.

4. Experimental measurements

4.1. Reflectance measurements

All samples were measured from 2 to 40 μm. In this work two different spectrophotometers have been used for the reflectance measurements. The choice of instrument depends on

different parameters such as surface roughness of the sample, type of desired reflectance measurement (total, specular or diffuse) and the actual wavelength region of interest.

For measurement of near normal specular reflectance, from 2 to 40 μm, a Perkin-Elmer 983 double-beam spectrophotometer was used. Evaporated gold mirrors were used as references. All samples were masked when measured since some of the alloy samples were smaller than the light spot of the spectrophotometer. The masks used were painted in black with a 15 mm circular opening placed in the centre of the light spot. The sample surfaces were placed on the masks and then measured. To compensate for the signal loss of the masks the sample reflectance, R_{sample}, was calculated according to

$$R_{\text{sample}} = 0.98\frac{R_{\text{mask+sample}} - R_{\text{mask}}}{R_{\text{mask+ref}} - R_{\text{mask}}} \tag{4}$$

where $R_{\text{mask+sample}}$ is the measured reflectance, R_{mask} is the reflectance of the mask without sample or reference mirror and $R_{\text{mask+ref}}$ is the reference reflectance measurement. The factor 0.98 is used to compensate for the reflectance of the gold mirrors. Since the PE-983 near normal reflectance accessory uses a relatively high incidence angle, s- and p-polarized light was measured separately to avoid polarization effects. The reflectance was obtained as the average of s- and p-polarized reflectance. For comparison, some of the alloy samples with larger surfaces were also measured without the masks. The reflectance results with and without mask were compared and differed by only a few tenths of one per cent. The accuracy in the measurements regarding systematic errors is less than 0.01.

To ensure that the polished samples were smooth and flat enough to be measured specularly in the PE-983, the samples were also measured in a spectrometer equipped with an integrating sphere. The instrument used was a Bomen Michelson 110 spectrometer, which is based on Fourier transform infrared spectroscopy. The instrument was equipped with an integrating sphere coated with gold. This instrument was used for reflectance measurements in the infrared wavelength range, from 2.5 to 20 μm, on all samples. The measurements were performed for near normal incidence. The size of the sample port of the integrating sphere is smaller than the polished surfaces of the samples so masking was not needed. The reference measurements were performed with an evaporated gold mirror. The comparison of the reflectance results from the two instruments, measured in the infrared wavelength range, showed no significant differences. From this we conclude that the samples were sufficiently polished. By using the instrument for specular reflectance we could extend the measurements to 40 μm instead of 20 μm, that is the maximum reached with the FTIR.

The near normal emittance at 10.5 μm was derived from the near normal reflectance data as $\varepsilon(10.5\ \mu\text{m}) = 1 - R(10.5\ \mu\text{m})$. The wavelength of 10.5 μm was chosen since it is the wavelength of maximal intensity for the blackbody radiation at 293 K. In order to limit the influence of noise in the measured data, the reflectance at 10.5 μm was derived from a linear fit between 10.2 and 10.8 μm. The standard deviation, s, was calculated from the measured data points, x_i, the linearly fitted value, $\langle x \rangle$, and the number of data points, n, according to

$$s = \sqrt{\frac{\sum_{i=1}^{n} (x_i - \langle x \rangle)^2}{n-1}}. \tag{5}$$

The standard deviation was calculated to 0.001 and marked in the figures as error bars.

The near normal thermal emittance, ε_{t}, was calculated as the average emittance weighted with the blackbody radiance distribution $I_{\text{b}}(\lambda, T)$ over the measured wavelength range, λ_1 to λ_2, for in this case T equal to the room temperature (293 K):

$$\varepsilon_{\text{t}} = \frac{\int_{\lambda_1}^{\lambda_2} (1 - R(\lambda)) I_{\text{b}}(\lambda, T)\, \text{d}\lambda}{\int_{\lambda_1}^{\lambda_2} I_{\text{b}}(\lambda, T)\, \text{d}\lambda}. \tag{6}$$

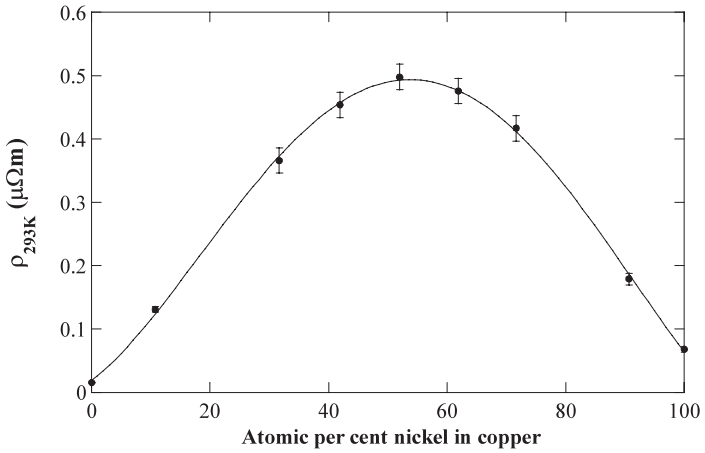

Figure 1. Resistivity versus composition at 293 K of copper–nickel alloys. The error bars mark the calculated maximum error for the resistivity measurements.

A calculation of the standard deviation is not necessary to perform in this case since the stochastical variation of the noise cancels out in the numerical integration routine.

4.2. Resistivity measurements

A standard four-probe method was used for the temperature dependent resistance measurements. The voltage was recorded in the temperature range 4.2–293 K with a Hewlett Packard 3457A multimeter instrument with an accuracy of 10^{-7} V at a constant current and data were sampled every second. The voltage of a platinum wire was calibrated to the temperature and used as a thermometer in the measurements. The sample thickness and width were measured with an accuracy of 0.05 mm. The source of error lies mainly in the measurements of the distance between the voltage wires connected to the sample. The distance between the two voltage wires was measured with an accuracy of 0.5 mm and used when calculating the resistivity of the samples. A maximum error analysis was performed for each sample and indicated as error bars in the figures.

5. Results and discussion

5.1. Resistance measurements

The resistivity of the copper–nickel alloys at 293 K can be seen in figure 1. The resistivity data show the typical behaviour with a maximum resistivity for slightly over 50% of nickel at ambient temperature (293 K), which is in good agreement with previously published data [22–24]. As a guide to the eye, the data are fitted to a four-degree polynomial; it was not possible to fit the data with a lower order polynomial. It is, however, possible to fit a straight line from pure copper to $Cu_{58}Ni_{42}$ in figure 1 with a slope that corresponds well to previous data [23]. The recorded resistivity versus temperature did not show any anomalous resistivity behaviour due to giant magnetic moments from atomic clustering of nickel in the magnetic phase as reported earlier [23, 25]. Sample preparation [26] and ageing effects [23] can play an important role in promoting atomic clustering. From this point it seems as if our samples were cluster free at the time of the measurements.

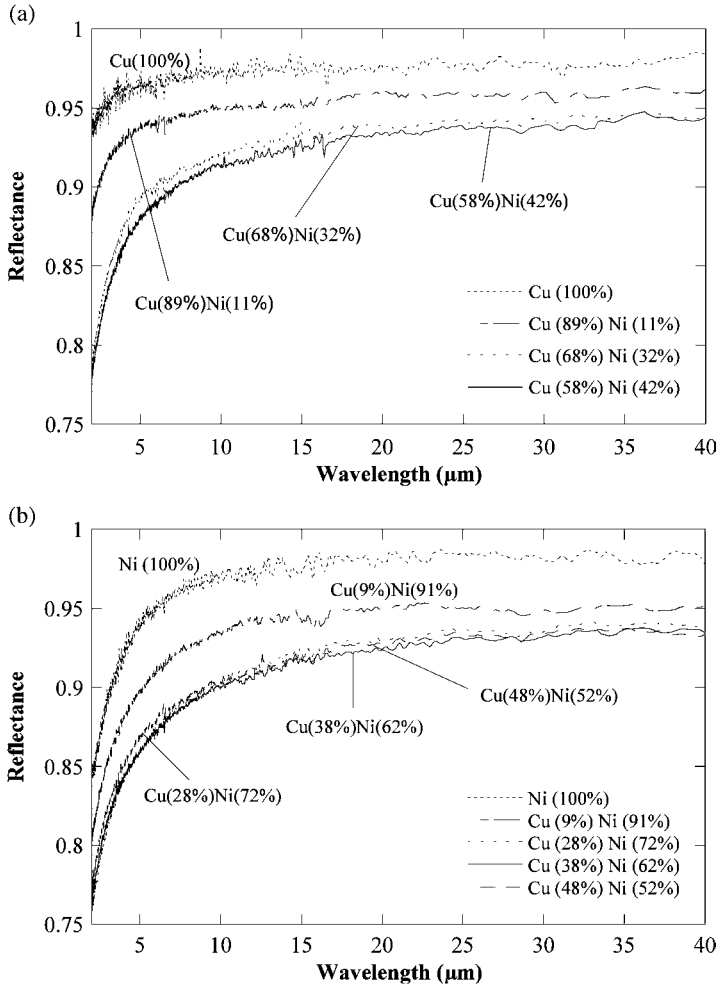

Figure 2. Reflectance versus wavelength of (a) copper-rich copper–nickel alloys and (b) nickel-rich copper–nickel alloys.

5.2. Reflectance measurements

The room temperature reflectance of the copper-rich Cu–Ni alloys can be seen in figure 2(a) and the nickel rich in figure 2(b). The reflectance of pure copper shows a high, fairly constant, reflectance from 5 to 40 μm. The reflectance of the copper-rich alloys is not 'copper-like' as the reflectance drops at shorter wavelengths to below 0.9 in the near infrared. This can be interpreted as interband transitions influencing the absorption in the near infrared wavelength range as reported previously [4]. With increasing nickel content the reflectance of the copper-rich alloys decreases over the whole measured range and between 20 and 40 μm the reflectance is fairly constant. Figure 2(b) shows the reflectance of the nickel-rich Cu–Ni alloys. The reflectance of the alloys is reduced compared to that of pure nickel. The wavelength dependence is very 'nickel-like' for the nickel-rich alloys as well. It is noticeable that the infrared reflectance for $Cu_{48}Ni_{52}$ is slightly higher than for $Cu_{38}Ni_{62}$. In the three samples with the highest copper

content a region with, except for the noise, fairly constant reflectance is found in a limited range between 30 and 40 μm.

The emittance of the Cu–Ni alloys at 10.5 μm is derived from the near normal reflectance in figure 2 and can be seen in figure 3(a). The emittance data points are, as a guide to the eye, fitted to a four-degree polynomial. The standard deviations of the measurements are marked as error bars.

The integrated emittance as defined in equation (6) is often of more practical use when evaluating thermal radiant properties of surfaces. We have therefore calculated the integrated emittance from equation (6) at 293 K, for all samples, which is shown in figure 3(b). The integrated emittance shows a similar dependence on alloy composition as the emittance at 10.5 μm. This is not surprising since the reflectance is fairly constant in the measured range.

Both the emittance at 10.5 μm and the integrated emittance for 293 K have a similar dependence on alloy composition as the resistivity but with the maximum value shifted from the sample with 52% Ni to 62% Ni.

5.3. Relation between the emittance and the resistance

In order to check the validity of the Hagen–Rubens relation in equation (3) the emittance at 10.5 μm was plotted versus the square root of the dc resistivity for all copper–nickel alloys. As seen in figure 4(a), a single line does not fit very well to all values, but if the data are divided in two groups, copper rich and nickel rich, it is seen that those two groups can be fitted to two linear curves that are almost parallel. Notice that the pure samples of copper and nickel are excluded from the fit since they do not fulfil the conditions for the Hagen–Rubens relation. For copper the Hagen–Rubens relation is only valid in the low frequency interval, i.e. $\omega\tau \ll 1$, and for nickel interband transitions dominate in the infrared wavelength region (see the introduction section).

The slope of the lines is compared to the constant factor in the Hagen–Rubens relation in equation (3). The constant has the value 0.115 $\mu\Omega^{-1/2}$ m$^{-1/2}$ for $\lambda = 10.5$ μm. The slope of both lines in figure 4(a) is 0.11 $\mu\Omega^{-1/2}$ m$^{-1/2}$.

In order to check whether we can also extend the validity of the Hagen–Rubens relation to the integrated emittance it has been plotted versus the square root of the resistivity in figure 4(b). As in figure 4(a), two linear curves are fitted, one for the copper-rich and one for the nickel-rich alloys. The values for pure copper and nickel are, in this case also, excluded from the fit. The slope is 0.11 $\mu\Omega^{-1/2}$ m$^{-1/2}$ for the copper-rich and 0.12 $\mu\Omega^{-1/2}$ m$^{-1/2}$ for the nickel-rich alloys. The Hagen–Rubens relation is not strictly valid for an integrated emittance. Therefore the same type of integration as in equation (6) was also performed on the right-hand side of equation (3), which from a mathematical point of view is formally correct:

$$\varepsilon_t = \frac{\int_{\lambda_1}^{\lambda_2} 2[\frac{4\pi\varepsilon_0 c\rho_0}{\lambda}]^{1/2} I_b(\lambda, T)\,d\lambda}{\int_{\lambda_1}^{\lambda_2} I_b(\lambda, T)\,d\lambda}. \tag{7}$$

The constant factor in this integrated version of the Hagen–Rubens relation then includes the integration of $\lambda^{-1/2}$ weighted by the blackbody radiation distribution. The constant factor for 293 K is 0.10 $\mu\Omega^{-1/2}$ m$^{-1/2}$, which is somewhat lower than the experimental values for the integrated emittance.

Based on earlier studies on electron structure from optical data and CPA calculations, one can expect a contribution to the emittance from interband transitions for the alloys, as mentioned in the introduction. However, the Hagen–Rubens relation seems to fit the data very well, that indicates that impurity scattering dominates. Considering the errors in the measurements, the

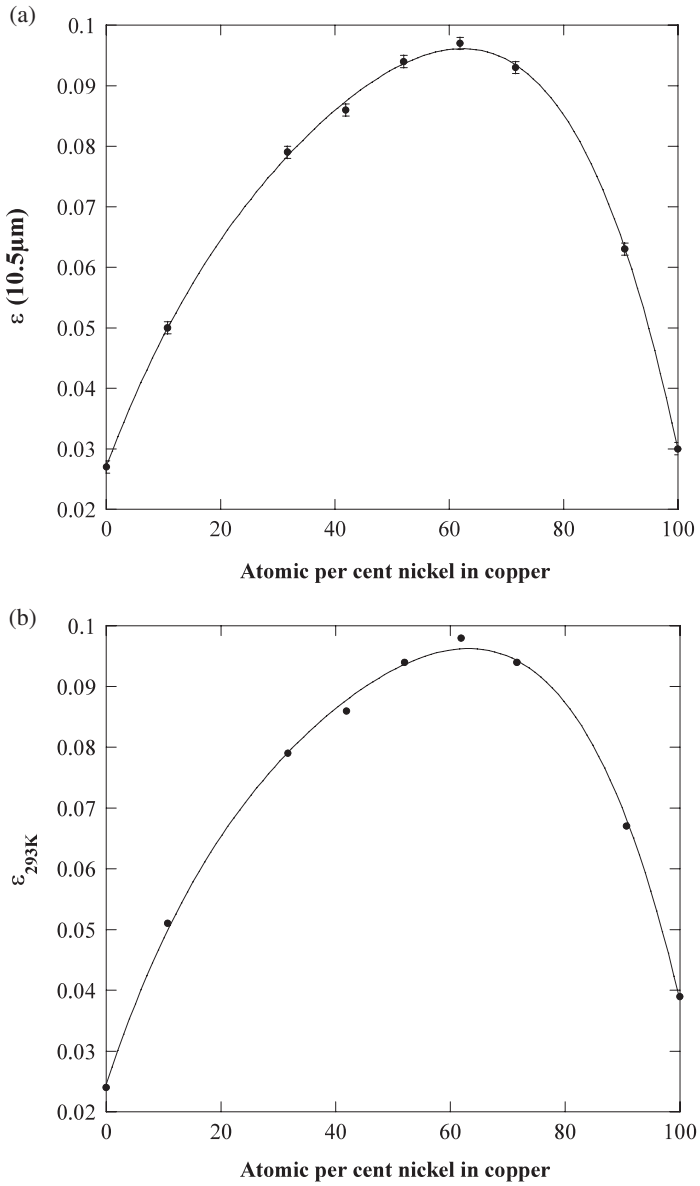

Figure 3. (a) Optical emittance, at 10.5 μm, versus composition of copper–nickel alloys. The standard deviation of is marked as error bars. (b) Thermal emittance at 293 K versus composition of copper–nickel alloys.

data fitted better to two parallel lines, none of them crossing zero emittance for zero resistance: one line for the copper-rich and the other for the nickel-rich alloys. This reflects the fact that the dc conductivity and the zero limit of the optical conductivity are different in some fundamental physical aspects as has also been observed before for pure metals [27]. It shows that the emittance has a constant contribution that is lacking in the resistivity. The emittance at zero resistivity is higher for the nickel-rich group than for the copper-rich group. Here we can only speculate and suggest that it may be at least partly due to interband transitions

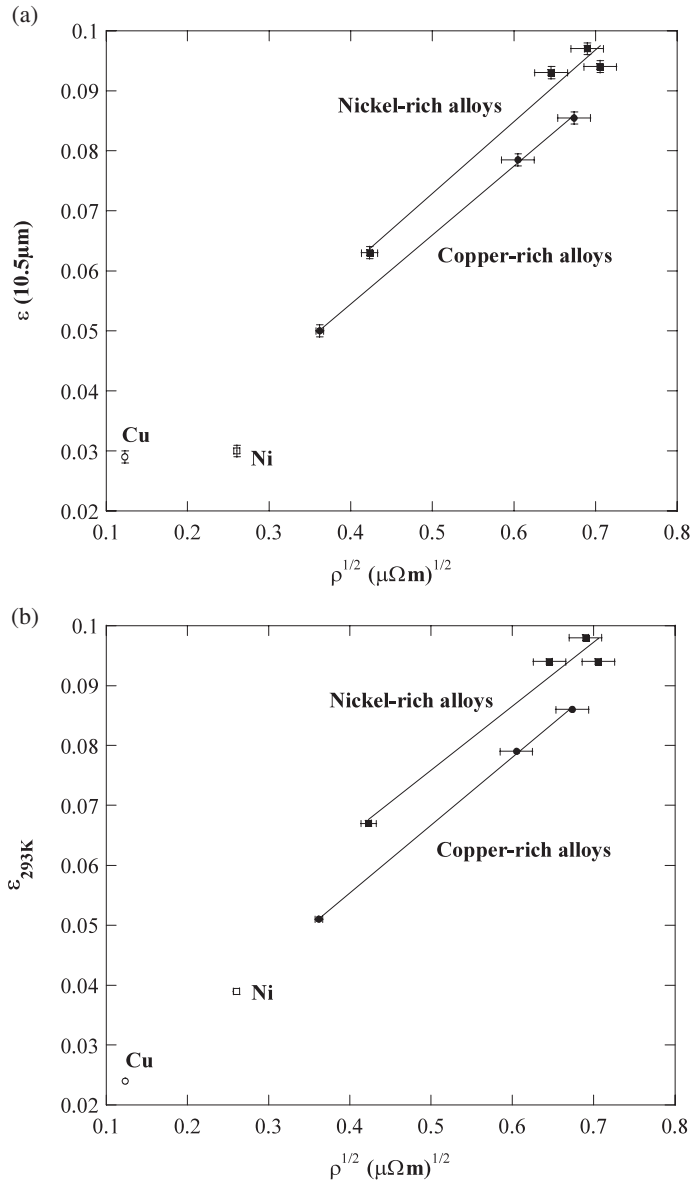

Figure 4. (a) Emittance at 10.5 μm versus square root of resisitivity at 293 K of copper–nickel alloys. A linear curve fit is included for the copper- and nickel-rich alloys. The horizontal error bars mark the maximum error of the square root of resisitivity at 293 K. The vertical error bars mark the standard deviation of the optical emittance. (b) Thermal emittance versus square root of resistivity at 293 K of copper–nickel alloys. A linear curve fit is included for the copper- and nickel-rich alloys. The horizontal error bars mark the maximum error of the square root of resisitivity at 293 K.

which is an optical phenomenon that has no coupling to the dc conductivity. It has been found from absorption measurements that the optical absorption at high energies (about 4 eV) is very similar within the group of copper-rich alloys including pure copper and within the nickel rich including pure nickel but different between the groups with higher absorption for

the nickel-rich group [18]. The character of the 'host' metal low energy bands is preserved also in the alloy. The higher emittance at zero resistivity for nickel-rich samples might then reflect the fact that interband transitions at higher energies are stronger in this group than in the copper-rich group.

6. Conclusions

The relation between emittance and atomic concentration in the Cu–Ni alloy follows a similar behaviour as the resistivity with a maximum emittance for nearly equal concentrations. The maximum value in resistivity is obtained for 52% Ni and in emittance for 62% Ni. The Hagen–Rubens relation can be established for both the copper-rich and nickel-rich samples with a very good agreement and is also supported by reports of short relaxation times in Cu–Ni alloys [3]. We therefore assume strong electron scattering from impurities so that intraband transitions dominate over interband transitions in the infrared wavelength range. The emittance is non-zero at zero dc resistivity, with a higher value for the nickel-rich samples, which we interpret as a contribution from interband transitions to the emittance. The shift in the concentration at maximum resistivity compared to maximum emittance might also have the same origin; the interband contribution to the emittance is higher for the nickel-rich samples compared to the copper rich and therefore shifts the curve to higher concentrations for the emittance. The validity of the Hagen–Rubens relation is confirmed and it can, as a good approximation, also be used for the integrated thermal emittance.

Acknowledgments

A number of people have been supportive during the progress of this work. Among others the authors would like to mention Nils-Olov Ersson, Jesper Edert, Anders Hoel, Arne Roos and Marie Wennström. This project was financially supported by the Bengt Ingeström Foundation and the Swedish National Energy Administration.

References

[1] Levy A, Barak G and Ashkenazi J 1987 *Phys. Rev.* B **35** 9474
[2] Mott N F and Jones H 1958 *The Theory of the Properties of Metals and Alloys* (New York: Dover)
[3] Beaglehole D 1976 *Phys. Rev.* B **14** 341
[4] Seib D H and Spicer W E 1970 *Phys. Rev.* B **2** 1676
[5] Seib D H and Spicer W E 1970 *Phys. Rev.* B **2** 1694
[6] Tokumoto M, Drew H D and Bagchi A 1977 *Phys. Rev.* B **16** 3497
[7] Kim K J and Lynch D W 1989 *Phys. Rev.* B **39** 9882
[8] Durham P J, Ghaleb D, Györffy B L, Hague C F, Mariot J-M, Stocks G M and Temmerman W M 1979 *J. Phys. F: Met. Phys.* **9** 1719
[9] Friedel J 1958 *Nuovo Cimento* **2** (Suppl.) 287
[10] Anderson P W 1961 *Phys. Rev.* **124** 41
[11] Schröder K and Önengut D 1967 *Phys. Rev.* **162** 628
[12] Stocks G M, Williams R W and Faulkner J S 1971 *Phys. Rev.* B **4** 4390
[13] Kirkpatrick S, Velicky B and Ehrenreich H 1970 *Phys. Rev.* B **1** 3250
[14] Munoz M C, Durham P J and Györffy B L 1982 *J. Phys. F: Met. Phys.* **12** 1497
[15] *Handbook of Optical Constants of Solids* 1985 (Orlando, FL: Academic)
[16] Drude P 1900 *Lehrbuch der Optik* (Leipzig: Hirzel)
[17] Lenham A P 1967 *J. Opt. Soc. Am.* **57** 473
[18] Sasovskaya I I and Noskov M M 1975 *Opt. Spectrosc.* **39** 64
[19] Beaglehole D and Kunz C 1977 *J. Phys. F: Met. Phys.* **7** 1923

[20] Kittel C 1996 *Introduction to Solid State Physics* 7th edn (New York: Wiley)
[21] Grosse P 1979 *Freie Elektronen in Festkörpern* (Berlin: Springer)
[22] Bozorth R M 1951 *Ferromagnetism* (Princeton, NJ: Van Nostrand-Reinhold)
[23] Legvold S, Peterson D T, Burgardt P, Hofer R J, Lundell B, Vyrostek T A and Gärtner H 1974 *Phys. Rev.* B **9** 2386
[24] *Handbook of Chemistry and Physics* 1992 73rd edn, vol 11 (Boca Raton, FL: CRC Press)
[25] Rossiter P L 1981 *J. Phys. F: Met. Phys.* 2105
[26] Clinton J R, Tyler E H and Lou H L 1974 *J. Phys. F: Met. Phys.* **4** 1162
[27] Lenham A P and Treherne D M 1966 *Optical Properties and Electronic Structure of Metals and Alloys* ed F Abeles (Amsterdam: North Holland)